Energy & Buildings 276 (2022) 112495

Contents lists available at ScienceDirect

Energy & Buildings

journal homepage: www.elsevier.com/locate/enb

Modeling and demand-based control of responsive building envelope with integrated thermal mass and active thermal insulations

Yawen He [a], Hongyu Zhou [a,⇑], Farbod Fahimi [b]

[a] Department of Civil and Environmental Engineering, University of Tennessee, Knoxville, TN 37996, USA
[b] Department of Mechanical and Aerospace Engineering, University of Alabama in Huntsville, USA

article info

Article history:
Received 8 August 2022
Revised 7 September 2022
Accepted 16 September 2022
Available online 21 September 2022

Keywords:
Responsive building envelope
Dynamic/active insulation
Control
Adaptive heat transfer

abstract

The static nature of current envelope design and operation is diametric to the mutable and transient forces and energies acting on our building stocks. Responsive building envelopes (or RBEs) have shown substantial energy saving potential for buildings by adaptively providing passive cooling/heating. In this research, an easy-to-implement yet flexible 'demand-based' control rule is proposed based on demand analysis to optimally control RBEs that integrate active insulation systems (AISs) and a sensible thermal energy storage (TES) layer. The controller developed herein calculates the desired thermal resistance for AIS layers and provides on-demand control of the heat flow into and out of the thermal mass to reduce AC load. It provides several benefits over the simple temperature-based controllers while does not require the complex formulation as needed for model predictive control. To quantify the thermal behavior and energy performance, a thermal network model is developed for RBEs to perform wholebuilding energy simulations of a residential thermal zone in six representative cities in the US. The results show apparent benefits of demand-based control strategy over traditional temperature-based control by offering higher energy savings and LPD reduction, especially in mild climate zones and during transitional seasons. Some design and implementation considerations for REBs with integrated AISs and TES are also discussed.

1. Introduction

The dynamic nature of forces and energies acting on the building structure has prompted the emergence of high-performance building skins that are interactive and responsive to the environment [1–6]. Responsive building envelopes (or RBEs) – also known as thermal dynamic building envelopes, are one of the approaches to achieve Net-zero energy buildings (Net ZEB) [7] and grid interactive efficient buildings (GEB), which has been an increasingly popular research topic in the past decade [8]. The core concept is to design buildings that could express similar responses to the ones found in plants, or that could imitate physiological responses of homeotherm animals like sweating or shivering [9]. In order to replicate such functionalities in buildings, RBEs rely on integrated technologies that are designed to enable the building to respond to a range of environmental stimuli such as temperature changes, using a combination of passive, active, and/or cognitive control strategies [2]. This design philosophy has a significant impact on the whole-building metabolism by enabling buildings to actively/semi-actively interact with its surrounding environment. By leveraging on-site renewable energy harvesting systems, it is possible to substantially reduce energy/operational cost, improve demand-side management, and occupant comfort [2,8,10,11].

The thermophysical properties of building envelopes are of great importance to reduce the energy consumption of buildings as the envelope is the main component separating building's interior spaces with the exterior environment. From an energy-saving perspective, high-insulation level (i.e., high R-value) is desired in cold climate zones with low internal gains level but has limited benefits during summer [12]. Similarly, envelopes with high insulation in hot climate zones provide marginal energy savings during transient and summer seasons [12]. Higher thermal mass is desired in temperate climate when thermal storage can be beneficial to improve thermal comfort and energy efficiency. High thermal mass is beneficial for residential buildings under hot humid climate during daytime but may increase building's energy use at night [13]. For the same reason, high thermal mass could have adverse impacts on building's energy efficiency in cold climates [14]. Ideally, the thermal properties of building envelopes should be attuned to the specific climate conditions to which they are subjected. However, due to the limitation on technologies, achieving

⇑ Corresponding author at: 851 Neyland Drive, 417 John D. Tickle Building, Knoxville, TN 37996-2313, USA.
E-mail addresses: hzhou8@utk.edu, hzhou8@utk.edu (H. Zhou).

https://doi.org/10.1016/j.enbuild.2022.112495
0378-7788/

Nomenclature

A	Area [m^2]
AIS	Active insulation system
AOF	Adaptive opaque façade
c_p	Specific heat [J/(Kkg)]
C	Heat capacity of node [J/K]
CV-RMSE	Coefficient of variation of the root mean square error
DIMs	Dynamic insulation materials
E	Heat from energy source [J]
F	View factor [−]
GA	Genetic algorithm
GEB	Grid interactive efficient building
h	Specific enthalpy [J/kg]
H	Heat transfer coefficient [W/K]
HVAC	Heating Ventilation and Air Conditioning
$I_s^{\#}$	Solar radiation incident [W/m^2]
LPD	Long-term percentage of dissatisfied [%]
m	Mass [kg]
MPC	Model-predictive control
N	Number of specified surfaces
Net ZEB	Net-zero energy building
NMBE	Normalized mean bias error
PCM	Phase change material
PMV	Predicted mean vote [−]
PPD	Predicted percentage of dissatisfied [%]
q	Heat rate [W/m^3]
Q	Heat rate [W]
R	Thermal resistance [$(Km^2)/W$]
RBE	Responsive building envelope
RSI	Thermal resistance with SI unit [$(Km^2)/W$]
SHGC	Solar heat gain coefficient [−]
t	Time [s]
T	Temperature [C]
TES	Thermal energy storage
TMY3	Typical meteorological year 3 weather data
U	Thermal transmittance [$W/(m^2K)$]
V	Differential control volume or finite control volume [m^3]
WWR	Window-to-wall ratio [−]
3R2C	Three resistors and two capacitors

Greek symbols

a	Solar absorptance [−]
e	Surface emissivity [−]
k	Heat conductivity [W/(mK)]
q	Density [kg/m^3]
r	Stephan-Boltzmann constant [$W/(m^2K^4)$]

Subscripts and superscripts

air_in	Indoor air
abs	Thermodynamic temperature
air_ex	Outdoor air
c	Cooling
des	Desired value
dmd	Demand
grd	Ground (long-wave radiation)
h	Heating
high	Upper limit
i,k,m,n	Numbering of surface node
inf	Infiltration
int	Internal gains
j	Numbering of time step
low	Lower limit
lw	Long-wave radiation
set	Set point
sky	Sky (long-wave radiation)
sys	Air conditioning system
sw	Short-wave radiation
th	Threshold value

variable insulation (i.e., variable R-value) has been the primary focus on current technology developments although there have been a few exploratory studies to investigate means to adjust/control the heat flow from and into the thermal mass of RBEs [15].

2. Background, research gaps, and objectives

Among the various RBE concepts, active insulation systems (AISs), or sometimes also been referred as to 'dynamic insulation materials (DIMs)' or adaptive opaque façade (AOF), are building envelopes with insulation materials that can actively change their thermal conductivity, which have been studied as one of the most promising RBE technologies so far to achieve building energy saving and improving occupant comfort. Early studies conducted by Krarti et al. [16,17] demonstrated that RBEs comprised of an AIS layer could lead to total energy savings ranging from 7 % to 42 % for residential buildings in different US climate zones. For these simulations by 3R2C models, the AIS layer was assumed to be able to change its thermal resistance (R-value) between two values, and its reaction was controlled using a simple temperature-based control approach [16,17]. In addition, Shekar and Krarti [18] investigated the use of a genetic algorithm (GA) based optimization approach to determine the optimal R-value setting for AISs. It was shown that depending on the building design, operation strategies and climatic conditions, the use of AIS with GA-optimized control may lead to 17 % of annual energy savings for US office buildings. When implemented as a roofing system [19], AIS has shown the ability to reduce up to 44 % energy used for space cooling, especially in mild climate and under heating dominated conditions. Further, Rupp and Krarti [20] compared several 'multi-step' control strategies – as oppose to the 'two-step' control used in most prior studies, for AISs in a residential building. A parametric analysis presented by the authors showed that more energy savings can be obtained by the multi-step control strategy in mild climates with relatively fewer cooling/heating degree-days; whereas RBE with simple ''on–off'' switchable insulation systems (i.e., with two settings: low and high R-value) would capture most of the cooling and heating savings that advanced dynamic insulation technologies that can vary their R-value continuously.

Although comprehensive, prior research on AISs as standalone building insulation systems did not fully leverage the energy-saving potential of RBE. To this end, Juaristi et al. [21] conducted a scoping study of over 15 RBE typologies for residential buildings situated in six different climate zones. The simulation results show that the RBE composed of an exterior AIS layer and a thermal mass layer provide higher energy savings than the one with an AIS layer sandwiched between two thermal mass layers. In addition, the pilot simulation study by Antretter et al. [22] and Mumme et al. [23] combined AISs with both sensible and latent thermal energy storage (TES) layers. In their study, different RBE layouts were studied where AISs were applied on exterior, interior, or both sides of a thermal mass layer. They performed EnergyPlus simulation using a DOE residential prototype building in eight selected climate zones. The results indicated that RBEs comprised of a thermal mass layer sandwiched between two AIS layers brought up to 71 %

energy use reduction while providing grid flexibility potential. Similar findings were concluded from the parametric studies conducted by Favoino et al. [24,25] for an office room extracted from a building in a temperate climate of Shanghai – RBEs comprised of a thermal mass layer sandwiched by two AISs attained maximum energy saving among all the configurations studied. All of these results indicated that AIS is effective in regulating the charging and discharging of thermal energy stored in thermal masses for effective heating/cooling load reduction. More recently, Kishore et al. [15] studied the energy performance of buildings with phase change materials (PCM) TES in combination with AIS. It was found that the PCM-AIS-integrated wall provides significantly higher energy saving potential than the AIS-only wall or the PCM-only wall in all the climates. Depending on the climate, the PCM-AIS-integrated wall could provide 15–72 % reduction in annual heat gain and 7–38 % reduction in annual heat loss [15]. The analysis presented in their study reinforces the need to combine scalable dynamic insulations with thermal energy storage systems for building energy saving.

Although previous research has encompassed understandings on the energy saving potential, benefits, and costs of responsive building envelope with AISs, existing control strategies did not fully explore the potential of AISs, particularly systems with AISs integrated with TES for enhanced energy saving. The majority of the research to date considered the R-value setting and HVAC operation separately [26]. Hence, the process of adjusting thermal resistances of AISs and HVAC control were decoupled. While this strategy had shown satisfactory performance with AISs acting as standalone insulations for buildings, its combination with TES adds complex dynamics where the different layers of AISs (i.e., exterior or interior) may be actuated at different time of the day/season to allow the thermal mass layer to charge (store) and release thermal energy when desired to either reduce or shed the peak AC loads. Due to the 'time-lag' effect brought by TES, a more sophisticated control strategy is required to achieve optimal performance of the system. To that end, Jin et al. [24,25] and Cui et al. [26] explored model-predictive control (MPC) as the control strategy for AISs and AISs-integrated TES building envelope. MPC has the advantages of being able to formulate and solve multiple optimization objectives, such as minimizing total energy consumption or operational cost [27], minimizing peak load demand [28], and minimizing the deviation between aggregated HVAC power consumption [29]. MPC is an appropriate choice for handling the slow moving process with time delays and therefore it is well-suited for simple and small systems [30].While effective, MPC requires the formulation of modeling, data collection, expert monitoring and deployment, which leads to higher design and deployment cost, especially for complex systems with large solution spaces [31]. In addition, it is hard for the controller to establish fixed model/rules and ensure high fidelity in a changing environment with high levels of variability [32].

To address these challenges, in this research an easy-to-implement yet flexible 'demand-based' control rule is formulated based on demand analysis to project the 'desired' thermal resistance of the AIS layers such that it beneficially utilizes the heat storage or precooling of the thermal mass to reduce AC load. In this research, a thermal network model is established for RBEs with integrated AIS and thermal energy storage (TES) to perform whole building energy simulations. A residential thermal zone having an RBE exterior walls is analyzed in six (6) climate zones – i.e., Miami, Phoenix, San Francisco, Albuquerque, Chicago, and Minneapolis, to quantify the thermal performance, energy saving potential, and thermal comfort improvement of TES-AIS integrated RBE with demand-based control. The performance of the newly developed demand-based control strategy is compared with temperature-based controllers. Some design and implementation considerations are discussed. Main innovative contribution of this work are:

1. Formulation of an easy-to-impalement demand-based control rule is presented for responsive building envelopes that combines AISs and sensible energy storage. In comparison to control strategies published in many previous studies, significantly higher energy saving potential has been achieved.
2. The thermal network model with high computational efficiency is established for RBEs with AIS and TES (or high thermal mass). The thermal performance (e.g., weekly temperature responses and energy consumptions) are compared to those obtained by EnergyPlus simulations. The higher computationally efficient model is important to reduce computational costs for further studies that employ AI-based or online learning control.
3. The control equation formulated here can calculate the desired R-value of the AIS based on the projected AC demands. This is important for AIS systems that are designed to change their thermal properties continuously, as oppose to the two stage 'on-and-off' control.
4. Traditional temperature rule-based control strategies tend to lead to overheating or overcooling during transitional seasons when applied to RBEs having high thermal mass or other forms of TES. The proposed demand-based control guarantees system performance by modulating thermal energy storage and release into and from the building envelope on demand. This also avoids unnecessary triggering of the AIS which reduces both operational and maintenance costs of the systems.
5. Detailed case studies are carried out for six climate zones in the US and conclusions are drawn regarding the applicability and design implications of RBEs.

3. Modeling of the building envelope with dynamic/active insulations

3.1. Thermal network model for integrated TES-AIS

In order to allow maximum flexibility in the implementation of AIS control, in this research a thermal network model based on a finite difference approach is established for building envelope with integrated TES and AIS systems. The 1-D heat transfer equation for any point with temperature T can be expressed as:

$$\frac{\partial(\rho h)}{\partial t} = \frac{\partial}{\partial x}\left(k\frac{\partial T}{\partial x}\right) + q_v \quad (1)$$

$$c_p = \frac{\partial h}{\partial T} \quad (2)$$

where t is time; ρ is material density; h is specific enthalpy; q_v is the rate of heat generated (or dissipated) within the material; c_p is material's specific heat.

Considering material's specific heat $c_p(t;T)$ and thermal conductivity $k(t)$ are variables as functions of time, Equation (1) can be rewritten as:

$$\rho c_p(t;T)\frac{\partial T}{\partial t} = k(t)\frac{\partial}{\partial x}\left(\frac{\partial T}{\partial x}\right) + q_v(t) \quad (3)$$

For a differential control volume, Equation (3) is expressed as:

$$\int_V \rho c_p(t;T)\frac{\partial T}{\partial t}dV = \int_V k(t)\frac{\partial}{\partial x}\left(\frac{\partial T}{\partial x}\right)dV + E_V \quad (4)$$

where V is volume and E_V is the rate of heat transferred from energy sources/sinks in this differential control volume.

Each layer of the RBE can be discretized into a number of finite volumes represented by a nodal network. Thus, finite difference method can be applied:

$$\rho_i c_{p,i}^{j} \frac{\delta T_i^{j+1} - T_i^{j}}{D t^{j}} \Delta x_i = \frac{1}{2}\left[q_i \frac{c_{p,i}^{j+1} \rho_{i-1}^{j+1} \delta T_{i-1}^{j+1} - c_{p,i}^{j} \rho_{i-1}^{j} \delta T_{i-1}^{j}}{D t^{j}} \Delta x_{i-1} \right] + q_i^{j} A = k_{i-1}^{j} \frac{T_{i-1}^{j} - T_i^{j}}{\delta x_{i-1}} A + k_i^{j} \frac{T_{i+1}^{j} - T_i^{j}}{\delta x_i} A + Q_i^{j} \quad (5)$$

where subscript i represents the nodal number; superscript j represents the j^{th} time step; A is surface area of the finite volume represented by node i; Q_i^j is the rate of heat transfer from energy sources in the finite volume of node i at j^{th} time step.

Equation (5) can be further rewritten as a general form for node i in a thermal network as:

$$C_i^{j} + \frac{1}{2} DC_i^{j} \quad T_i^{j+1} - T_i^{j} = H_{i-1,i}^{j} T_{i-1}^{j} + H_{i+1,i}^{j} T_{i+1}^{j} - \left(H_{i-1,i}^{j} + H_{i+1,i}^{j} \right) T_i^{j} + Q_i^{j} \Delta t^{j} \quad (6)$$

where C_i^j is the thermal capacitance of node i at j^{th} time step; $H_{i-1,i}^j$ is the heat transfer coefficient representing conduction between node i-1 and node i with variable thermal properties at j^{th} time step:

$$\begin{aligned} C_i^{j} &= \rho_i c_{p,i}^{j} \Delta x_i A \\ DC_i^{j} &= \rho_i \left(c_{p,i}^{j+1} - c_{p,i}^{j} \right) \Delta x_i A \\ H_{i-1,i}^{j} &= k_{i-1}^{j} \frac{A}{\delta x_{i-1}} \\ H_{i+1,i}^{j} &= k_{i+1}^{j} \frac{A}{\delta x_i} \end{aligned} \quad (7)$$

For a AIS with negligible thermal mass [16,33–40], it can be represented by a 'no-mass layer' consisting of two nodes – one capture the convective and radiant heat transfer from the exterior environment, while another connected to the internal nodes for conduction. Thus, the AIS with negligible thermal mass in a thermal network may be represented as:

$$H_{i-1,i}^{j} + H_{i+1,i}^{j} \quad T_i^{j} = H_{i+1,i}^{j} T_{i+1}^{j} + H_{i-1,i}^{j} T_{i-1}^{j} + Q_i^{j} \quad (8)$$

where the time-varying the heat transfer coefficient $H_{k,i}$ between node k and node i with variable insulation at time t^j can be adjusted to regulate the amount of heat flow into indoor space. In different AIS design, the heat transfer coefficient can either be idealized as a binary function where its insulation value 'switches' between two values (Equation (9)) or a gradually variable of the environmental stimuli (Equation (10)):

$$H_{k,i}^{j} = f_{binary}\left(t^{j}; T_i^{j}; Q_i^{j} \right) = \begin{cases} H_{high} & \text{criterion 1} \\ H_{low} & \text{criterion 2} \end{cases}^{k,i} \quad (9)$$

$$H_{k,i}^{j} = f_{continous}\left(t^{j}; T^{j}; Q^{j} \right) \quad (10)$$

In this study, an RBE layout is selected where a high thermal mass concrete layer is sandwiched between two AIS layers as shown in Fig. 1, to maximize load shifting capabilities of the RBE. In this configuration, the thermal resistances (R-values) of the exterior and interior AISs can be separately controlled [22]. During the heating season, the thermal resistance of the exterior AIS layer can be lowered when the outdoor air temperature is higher than the temperature of the thermal mass to allow the thermal mass to be 'charged'; otherwise, the exterior AIS is switched to 'insulative' mode to minimize heat loss of the concrete thermal mass. For a given moment when heating is needed and the temperature of the thermal mass is higher than that of the indoor air, the thermal conductivity of interior AIS can be increased to offset the AC system demand. The same logic applies to the cooling season to discharge/precool the thermal mass when outdoor air temperatures are lower than the thermal mass while utilizing the 'precooled' thermal mass to reduce cooling load. This design has been proved more effective than other layouts in previous studies [22,25]. Since this RBE layout combines the benefits of active insulation (AIS) and thermal energy storage (TES), it is also referred as to TES-AIS integrated RBE [15,23].

For this TES-AIS configuration, considering the heat flow from short-wave radiation$Q_{1;sw}^j$, long-wave radiation $Q_{1;lw}^j$ and convection acting on the exterior AIS (opaque, no solar transmission), Equation (8) can be rewritten as:

$$H_{air\_ex;1}^{j} + H_{2;1}^{j} \quad T_1^{j} = H_{2;1}^{j} T_2^{j} + H_{air\_ex;1}^{j} T_{air\_ex}^{j} + Q_{1;sw}^{j} + Q_{1;lw}^{j} \quad (11)$$

$$Q_{1;sw}^{j} = a_1 I_{s;1}^{\#;j} A_1 \quad (12)$$

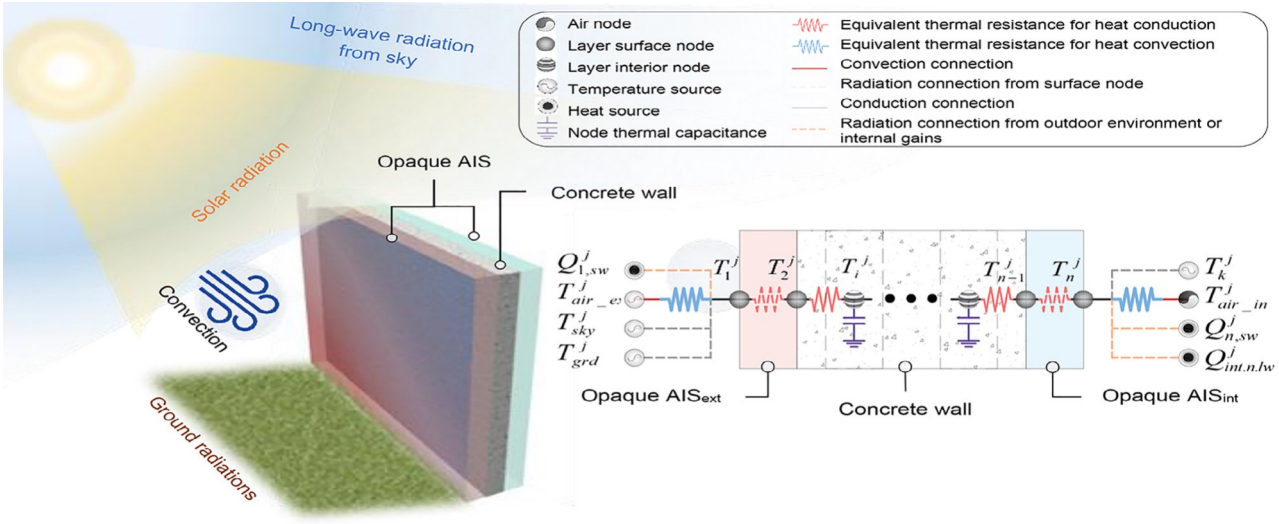

Fig. 1. Nodal scheme of the integrated AIS-TES responsive building envelope.

$$Q^{j}_{1;lw} = \left\{ \begin{array}{l} F^{sky}_{1}\left(T^{j}_{sky;abs}{}^{4} - T^{j}_{1;abs}{}^{4}\right) + F^{grd}_{1}\left(T^{j}_{grd;abs}{}^{4} - T^{j}_{1;abs}{}^{4}\right) \\ + F^{air\_ex}_{1}\left(T^{j}_{air\_ex;abs}{}^{4} - T^{j}_{1;abs}{}^{4}\right) \\ + \varepsilon_1 A_1 - \sum_k \varepsilon_k F_k \left(T^{j}_{k;abs}{}^{4} - T^{j}_{1;abs}{}^{4}\right) A_k \end{array} \right\} \quad (13)$$

where $H^{j}_{2;1}$ is heat transfer coefficient at j^{th} time step between node 1 (exterior surface of AIS) and node 2 (exterior surface of the concrete layer) – $H^{j}_{2;1}$ is a time variant determined by the control sequence; α_1 is constant solar absorptance of exterior active insulation surface. F^{k}_{1} is the view factor for node 1 with exterior emitting surface k – i.e., wall or window surfaces; other notations in the equations are listed in the nomenclature.

The interior surface node considers short-wave radiation from lighting ($Q^{j}_{light;n;sw}$), long-wave radiation from occupant activities, lighting and equipment ($Q^{j}_{people;n;lw}$; $Q^{j}_{light;n;lw}$; $Q^{j}_{equip;n;lw}$). Thus, the heat balance equation for interior surface node can be expressed as:

$$H^{j}_{n1;n}\left(H^{j}_{air\_in;n} - T^{j}_{n}\right) = H^{j}_{n1;n}T^{j}_{n1} + H^{j}_{air\_in;n}T^{j}_{air\_in} + Q^{j}_{n;sw} + Q^{j}_{n;lw} \quad (14)$$

$$Q^{j}_{n;sw} = \alpha_n I^{\#;j}_{s;n} A_n + Q^{j}_{light;n;sw} \quad (15)$$

$$Q^{j}_{n;lw} = \sum_k \varepsilon_n F^{k}_{n}\left(T^{j}_{k;abs}{}^{4} - T^{j}_{n;abs}{}^{4}\right) A_k + Q^{j}_{people;n;lw} + Q^{j}_{light;n;lw} + Q^{j}_{equip;n;lw} \quad (16)$$

The heat balance equation for the thermal node at AIS-concrete interface and the internal nodes within the concrete wall layer follows the formulation of typical mass wall as:

$$C_i T^{j+1}_{i} = C_i T^{j}_{i} + H^{j}_{i1;i}T^{j}_{i1} + H^{j}_{i+1;i}T^{j}_{i+1} - H^{j}_{i1;i}H^{j}_{i+1;i}T^{j}_{i} + Q^{j}_{i}\Delta t^{j\,j} \quad (17)$$

3.2. Validation of the thermal network model

To validate the thermal network model for the whole-building energy analysis with the RBE, simulations were performed on a single room house as shown in Fig. 2, and the results were compared to those obtained from EnergyPlus simulations. The house has an RBE with 15 %window ratio on its south side exterior walls, floor and roof. The dimension of the single-room building is 13 m (L) 8 m (W) 3.05 m (H). The RBE consists of a 100-mm thick concrete layer sandwiched between two opaque AIS layers with (R_{low} = 0.01 Km^2/W and R_{high} = 1.5 Km^2/W). The RSI-values of other exterior walls, floor, and roof are enlisted in Fig. 2 according to ASHRAE 90.1. Typical meteorological year 3 (TMY3) weather data of San Francisco is used for the simulation. The U-value of the glazing is 2.0 W/(K m^2). The window solar heat gain coefficient (SHGC) is 0.1, which is complaint with ASHREA-90.1 [41] and within the available range according to NFRC [42]. The solar absorptance of all the walls was 0.7 and the surface emissivity of all the walls was 0.9, which are commonly used [43]. The indoor air temperature was controlled by constant air volume (CAV) HVAC system with dual setpoints of 21.1–23.9 C. The selection of this neutral band is based on prior research [44]. The other simulation details are enlisted in Fig. 2(a).

For the thermal network model, the heat balance of indoor air considers convective heat exchange with interior wall and window surfaces, air conditioning, infiltration, and absorption of heat from internal gains generated by occupant activity, lighting, and equipment. The influence from air conditioning, infiltration and human activity for the moisture balance of indoor air were also considered whereas the influence of moisture on wall thermal properties are neglected. The 3-D heat transfer process of a thermal zone was represented by assembling a nodal network that represents the interactions among all the wall layer nodes and air nodes following a general approach proposed by Kim et al. [45]. Detailed formulations for the building envelope, interior partitions, and indoor air represented by a nodal network for a single-zone building can be found in the previous work of the authors [46]. In numerical computation, long-wave radiation is linearized using the same method as detailed in [47]. Simple glazing system model [48] was used for windows in this building model, where window layer is assumed as no-mass layer. At each time step, heat balance and moisture balance of indoor air were computed separately.

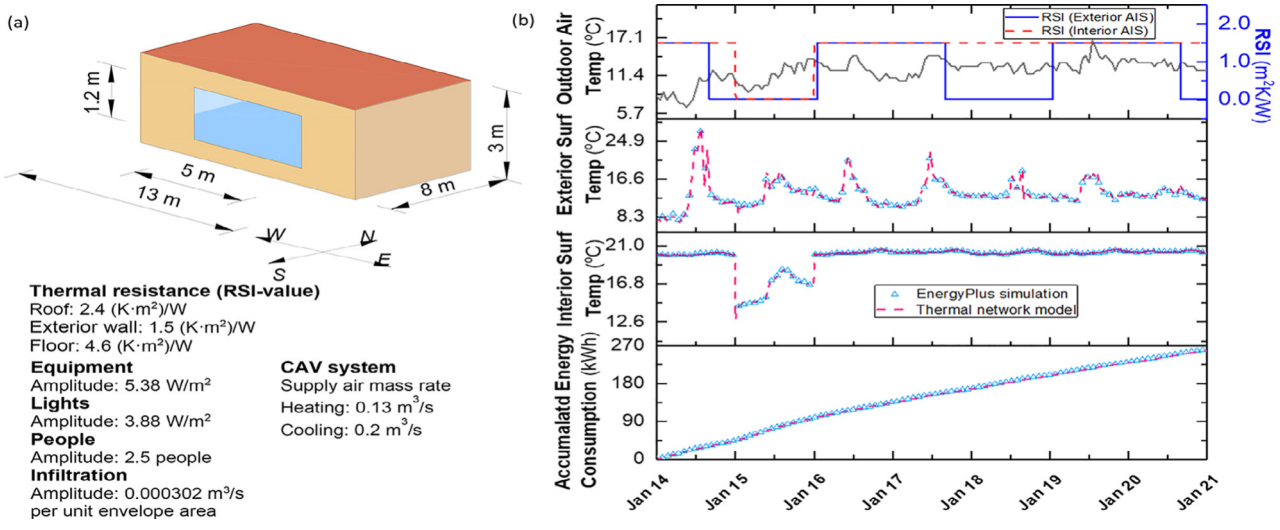

Fig. 2. (a) Isometric view of the building modeled for calibration; (b) Comparison of the simulation results between thermal network model and EnergyPlus.

Fig. 2(b) presents the outdoor air temperature, RSI-value settings of the exterior and interior AISs, and the simulated surface temperatures, as well as the indoor air temperature obtained by both the thermal network and EnergyPlus models. It can be seen that the simulation results match closely. The CV-RMSE (coefficient of variation of the root mean square error) and NMBE (normalized mean bias error) of energy consumption (district heating or cooling) are calculated at 3.6 %and 1.5 %, respectively, which are both well under the ASHRAE Guideline 14 [49] (i.e., <30 %CV-RMSE and <10 %NMBE for hourly data), indicating acceptable accuracy of the thermal network model.

4. Demand-based control for responsive building envelope

In this section, an easy-to-implement yet flexible 'demand-based' control rule is formulated for the TES-AIS integrated RBEs to beneficially utilize the heat storage or precooling of the thermal mass to reduce AC load. Since the sensible AC load for a thermal zone is mainly attributed to: (1) the convective heat exchange between indoor air with interior walls and window surfaces, (2) infiltration, and (3) internal gains from occupant activity, lighting, and equipment [48], the control rule for AIS is formulated based on the AC demand approximated from estimated internal gains, infiltration, as well as measured surface temperatures and air temperatures, see Fig. 3. For simplicity, the control rule formulation is based on a single thermal zone while it can be extended to a multi-zone scenario via distributed control strategies with a decentralized law [50,51]. More detailed control formulation for a multi-zone building with RBEs worth further investigation and is beyond the scope of this paper. The heat balance on the zone air for a single thermal zone is:

$$C^{j}_{air\_in}\frac{DT^{j}_{air\_in}}{Dt^{j}} = Q^{j}_{air\_in;int} + Q^{j}_{air\_in;inf} + \sum_{i}^{N_{surfaces}} H^{j}_{i;air\_in}\left(T^{j}_{i} - T^{j}_{air\_in}\right) + Q^{j}_{sys} \quad (18)$$

where $C^{j}_{air\_in}$ is the thermal capacitance of indoor air node at the j^{th} time step; $H^{j}_{i;air\_in}$ is the heat transfer coefficient between surface node i and indoor air node; $N_{surfaces}$ is the number of wall surfaces; Q^{j}_{sys} is the HVAC system output; $Q^{j}_{air\_in;int}$ and $Q^{j}_{air\_in;inf}$ are convective heat gain from internal loads and infiltration, which can be expressed as [48]:

$$Q^{j}_{air\_in;int} = Q^{j}_{people;air\_in;conv} + Q^{j}_{light;air\_in;conv} + Q^{j}_{equip;air\_in;conv} \quad (19)$$

$$Q^{j}_{air\_in;inf} = c_{p;air\_in}\dot{m}^{j}_{air\_in;\,inf}\left(T^{j}_{air\_ex} - T^{j}_{air\_in}\right) \quad (20)$$

For each control step j, for time interval Dt^{j}, the system output demand $Q^{j}_{sys}(T^{j}_{set})$ to reach the setpoint T^{j}_{set} can be written as:

$$Q^{j}_{sys;dmd}(T^{j}_{set}) = C^{j}_{air\_in}\frac{T^{j}_{set} - T^{j}_{air\_in}}{Dt^{j}} + \sum_{m}^{N_{surface}} H^{j}_{m;air\_in}\left(T_{m}{}^{j} - T^{j}_{air\_in}\right) - Q^{j}_{air\_in;int} - Q^{j}_{air\_in;inf} \quad (21)$$

If one of the exterior surfaces is an RBE. Under cooling mode, when the thermal mass (concrete) has lower temperature than the indoor air ($T^{j}_{n1} < T^{j}_{air\_in}$), we suppose that all or a portion of the system output demand to reach the setpoint $Q^{j}_{sys;dmd}(T^{j}_{set})$ is compensated by the beneficial heat flow from the RBE, Equation (21) becomes:

$$Q^{j}_{sys;dmd}(T^{j}_{set}) + H^{j}_{n;air\_in}\left(T^{j}_{n} - T^{j}_{air\_in}\right) = C^{j}_{air\_in}\frac{T^{j}_{set} - T^{j}_{air\_in}}{Dt^{j}} + \sum_{m}^{N_{surface}-1} H^{j}_{m;air\_in}\left(T^{j}_{m} - T^{j}_{air\_in}\right) - Q^{j}_{air\_in;int} - Q^{j}_{air\_in;inf} \quad (22)$$

where T^{j}_{n} is the interior surface temperature of the RBE; $H^{j}_{n;air\_in}$ is the heat transfer coefficient between the RBE interior surface and the indoor air. In an ideal case when all of $Q^{j}_{sys;dmd}$ can be supplied by the desired convective heat transfer from the RBE –

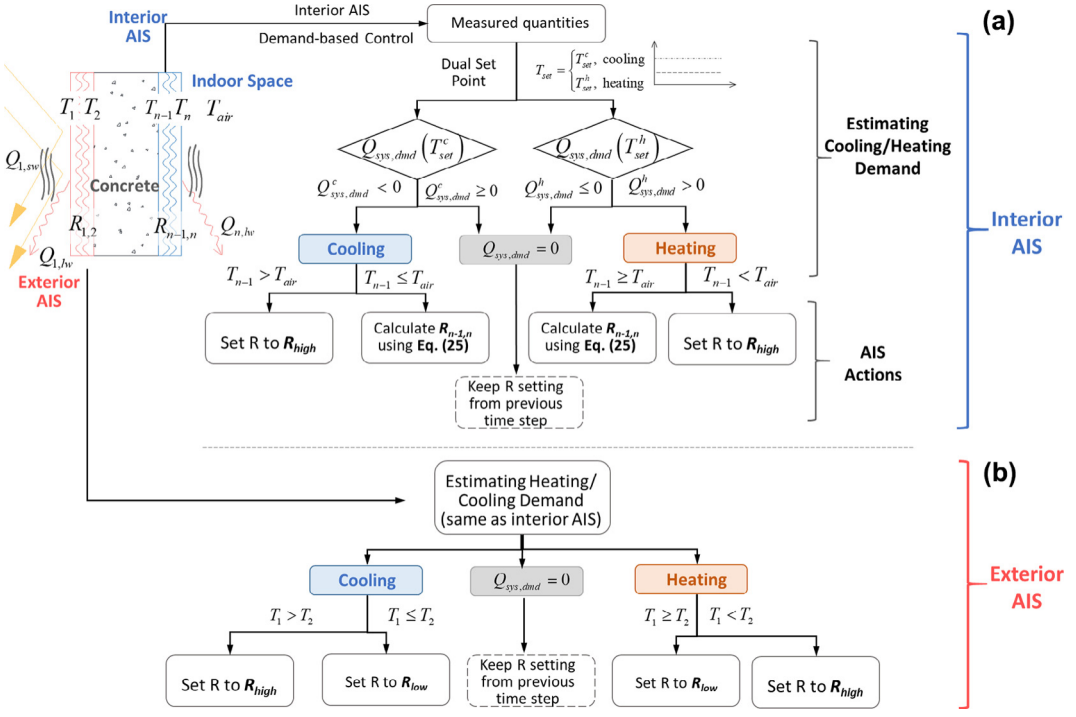

Fig. 3. Control rule for building envelope with AISs and one concrete layer: (a) control rule for interior AIS; (b) control rule for exterior AIS.

i.e.,$Q^{j}_{sys;dmd} = 0$, and consider the heat balance of the RBE interior surface node (Fig. 1):

$$H^{j}_{n;air\_in}\left(T^{j}_{n} - T^{j}_{air\_in}\right) = \frac{A_n}{R^{j}_{n1;n}}\left(T^{j}_{n1} - T^{j}_{n}\right) + Q^{j}_{n;sw} + Q^{j}_{n;lw} \quad (23)$$

where T^{j}_{n1} is temperature at the concrete interior AIS interface; A_n is the interior surface area. Equation (22) becomes:

$$\frac{A_n}{R^{j}_{sys;dmd}}\left(T^{j}_{n1} - T^{j}_{n}\right) = C_{air\_in}\frac{T^{j}_{set} - T^{j}_{air\_in}}{Dt^{j}} + \sum_{m}^{N_{other}} H^{j}_{m;air\_in}\left(T^{j}_{m} - T^{j}_{air\_in}\right) + Q^{j}_{irr;int} + Q^{j}_{air\_in;inf} + Q^{j}_{n;sw} + Q^{j}_{n;lw} \quad (24)$$

$R^{j}_{n1;n}\big|_{Q^{j}_{sys;dmd}=0}$ is the desired thermal insulation level of the interior AIS to achieve $Q^{j}_{sys;dnd}$. Rewriting Equation (24) and consider the physical limits of the AIS thermal resistance, we have:

$$R^{j}_{n1;n}\big|_{Q^{j}_{sys;dmd}=0} = \max\left[\frac{T^{j}_{n1} - T^{j}_{n}}{Q^{j}_{RBE;des} + Q^{j}_{n;sw} + Q^{j}_{n;lw}}A_n;\ R_{low}\right] \quad (25)$$

where $Q^{j}_{RBE;des}$ is the ideal (desired) heat flow from AIS to offset HVAC load, which can be written as:

$$Q^{j}_{RBE;des} = C^{j}_{air\_in}\frac{T^{j}_{set} - T^{j}_{air\_in}}{Dt^{j}} + \sum_{m}^{N_{other}} H^{j}_{m;air\_in}\left(T^{j}_{m} - T^{j}_{air\_in}\right) + Q^{j}_{air\_in;int} + Q^{j}_{air\_in;inf} \quad (26)$$

where R_{low} is the lowest thermal resistance of AIS limited by its materials and design.

When $T^{j}_{n1} > T^{j}_{air\_in}$ and under cooling mode, the Rvalue of interior AIS is set to R_{high} to minimize the undesired heat flow from the thermal mass layer to indoor space, see Fig. 3. Similarly, under heating mode and when the thermal mass layer can provide beneficial heat flow to the indoor space ($T^{j}_{n1} > T^{j}_{air\_in}$), the thermal resistance of interior AIS can be calculated using Equation (25), otherwise ($T^{j}_{n1} < T^{j}_{air\_in}$) the thermal resistance of interior AIS will be set to R_{high}. The detailed control sequence is shown in Fig. 3.

The proposed control sequence will enable the RBE to provide on-demand heat flow to help reaching a specific indoor air setpoint while minimizing AC demand. To achieve this, AISs with continuously adjustable thermal resistance (e.g., variable pressure VIP [52] and adaptive multi-layer insulation [40]) may provide benefit over the 'two-step' control (RSI-value can be switched only between R_{high} and R_{low}) [20].

The thermal resistance setting of exterior AIS is dictated by the 'charging/discharging' needs of the thermal mass layer – i.e., under cooling mode, when the concrete temperature T^{j}_{2} is greater than the exterior AIS surface temperature T^{j}_{1}, the thermal resistance of exterior AIS $R^{j}_{1;2}$ is set to R_{low}; otherwise $R^{j}_{1;2}$ is set to R_{high}. Likewise, under heating mode, if $T^{j}_{2}<T^{j}_{1}$, $R^{j}_{1;2}$ is set to R_{low}; otherwise $R^{j}_{1;2}$ is set to R_{high}, see Fig. 3.

5. Csase studies

5.1. Simulation details

To study the thermal behavior and energy saving potential of the RBE, the thermal network model as described in Section 3.1 is implemented to model a single 13 m (L) 8 m (W) 3.05 m (H) exterior thermal zone extracted from an intermediate floor of an apartment building. The exterior wall exposed to outdoor environment is assumed to be either RBE or an ASHREA-90.1 compliant standard wall in the baseline case for comparison. All internal walls are assumed to be adiabatic [25]. The window-to-wall ratio is 15 %for the exterior wall. Some other wall properties (e.g., window U-value, window SHGC, solar absorptance and surface emissivity of walls) and simulation parameters considered include occupant activities, lighting, equipment schedules, and infiltration level as listed in Fig. 4. RBEs described in Section 3.1 are used for the case study – i.e., a concrete (thermal mass) layer sandwiched between two opaque AISs as shown in Fig. 1. The RSI-value range of exterior or interior AIS is assumed to be R_{low} (0.1 Km^2/W) to R_{high} based on the thermal resistance range reported in prior literature [17,21,23,41]. To provide comparisons of the thermal behavior and energy performance of RBE as compared to the static baseline, a baseline exterior wall is designed with the same layout as RBE where a concrete mass layer is sandwiched between two rigid foam insulation panels with the same overall thermal mass and thermal resistance (or the upper limit for RBE with AISs) as the RBE cases. The thermal resistance of the baseline wall (static) and the R_{high} of RBE are set based on the RSI-value enlisted in Fig. 4 for different climate zones in accordance with ASHREA 90.1.

For the simulation, it is also assumed that the long-wave absorptivity and long-wave emissivity are the same for all wall surfaces. Typical meteorological year 3 (TMY3) weather data of 6 representative climate zones (Miami, Phoenix, San Francisco, Albuquerque, Chicago and Minneapolis) were used for the simulation. The indoor air temperature was controlled by HVAC with dual setpoints of 21.1–23.9. The Predicted Mean Vote (PMV) and Predicted Percentage of Dissatisfied (PPD) based on Frager's model [53] are used to evaluate thermal comfort-time performance of the building. The Long-term Percentage of Dissatisfied (LPD) is used to assess occupants' long-term thermal comfort [54].

5.2. Results and discussion

5.2.1. Heating season

Fig. 5 shows the thermal behavior of the RBE during heating season. Seven days' (January 3th–10th) data in Chicago, IL (ASHREA climate zone 5A) are arbitrarily chosen to illustrate the thermal behavior and AIS operations of the RBE during the heating season. Fig. 5(a) shows the outdoor air temperature and estimated system output demand $Q^{j}_{sys;dmd}$ to reach the setpoint, as calculated using Equation (21) and according to the flowchart shown in Fig. 3. During the winter months, the AC is in heating mode during most days. Fig. 5(b) shows that the temperature of concrete thermal mass is always lower than the indoor air temperature during this period, the interior AIS therefore remains at high thermal resistance mode (R_{high}) to minimize the heat loss from the indoor space. As shown in Fig. 5(c), when the exterior surface temperature is higher than the concrete temperature, the thermal resistance (RSI-value) of the exterior AIS is set to R_{low} to allow beneficial heat flow to charge/heat the concrete thermal mass. Otherwise, the RSI-value of the exterior AIS is set to R_{high} to minimize the heat loss from the concrete. This dynamic behavior of exterior AIS helps to maintain a relatively low temperature difference between the concrete layer and the interior surface, thus reducing the heat loss. In a heating dominant case where the exterior surface temperature is mostly lower than the heating setpoint, RBE provides limited (if at all) energy saving potential. This is consistent with prior studies [17,20].

5.2.2. Cooling season

Fig. 6 shows the thermal behavior and operation of the interior and exterior AISs for the RBE wall during the cooling season, where

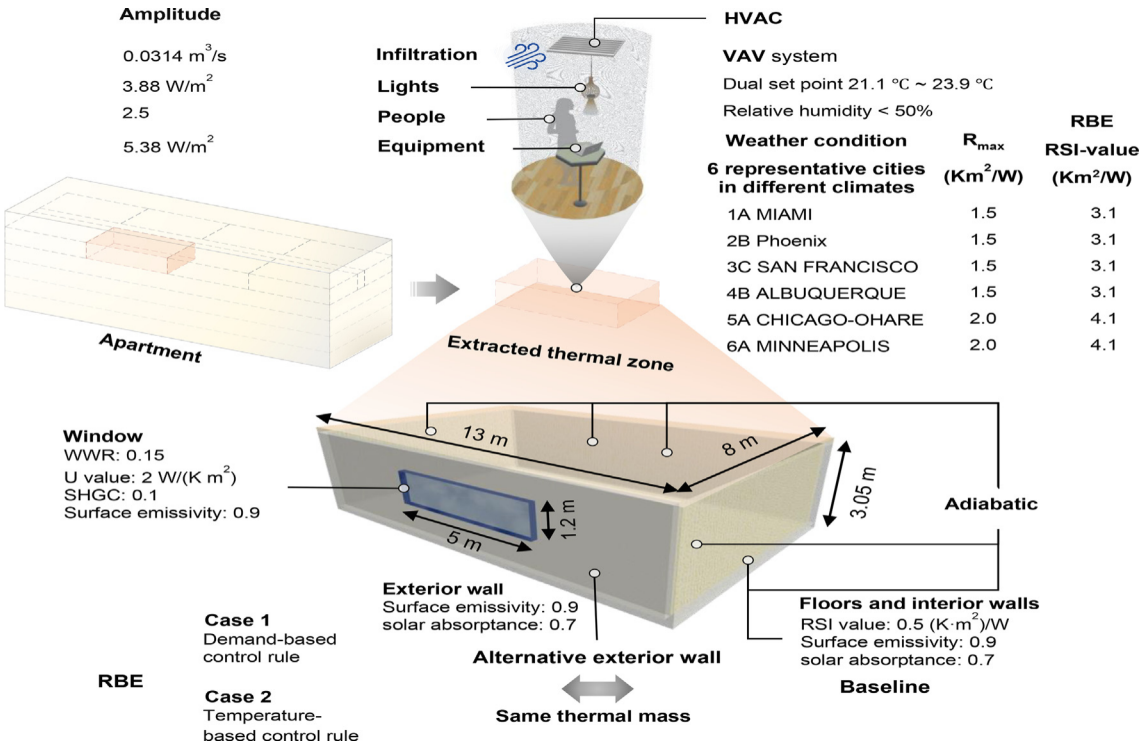

Fig. 4. Simulation details for a residential thermal zone with RBE in comparison with a baseline static envelope.

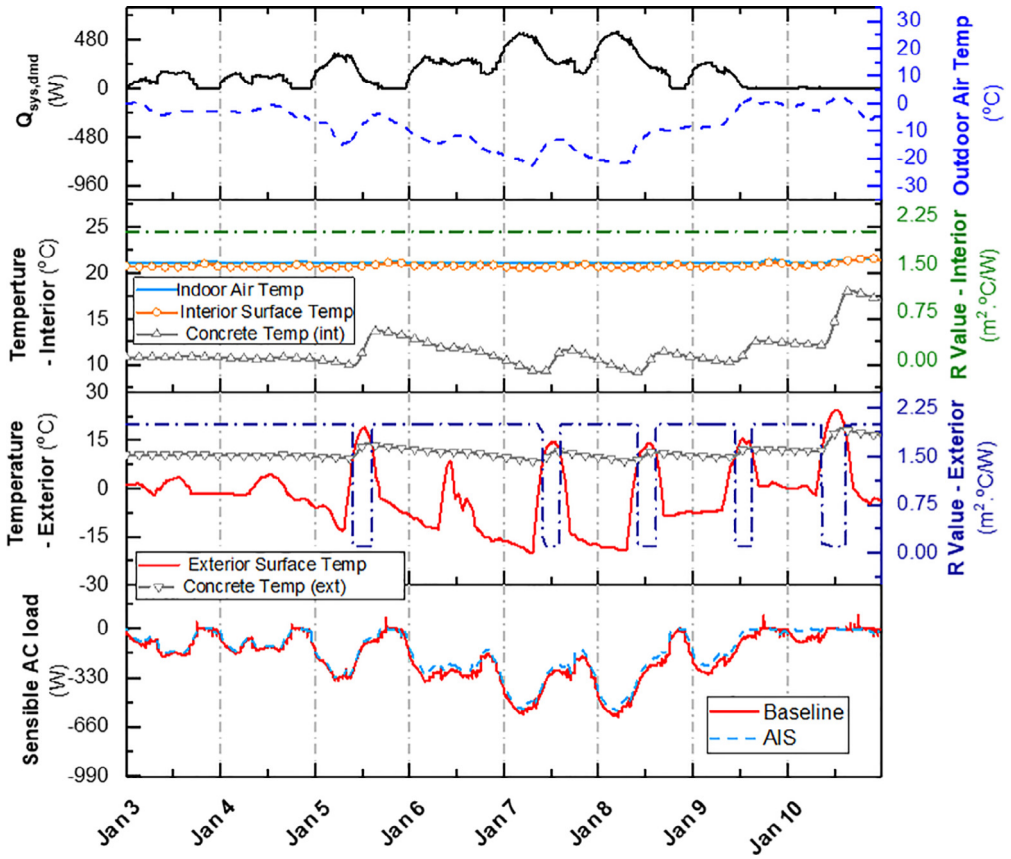

Fig. 5. Thermal behavior of RBE in a typical heating season (January, Chicago, IL): (a) outdoor air temperature and the system output demand to reach the setpoint, $Q_s y_{s;dmd}$(Equation (21)); (b) interior AIS R-value setting and indoor air, interior surface and concrete temperatures; (c) exterior AIS R-value setting, exterior surface and concrete temperatures; (d) comparison of sensible AC load for RBE and baseline cases.

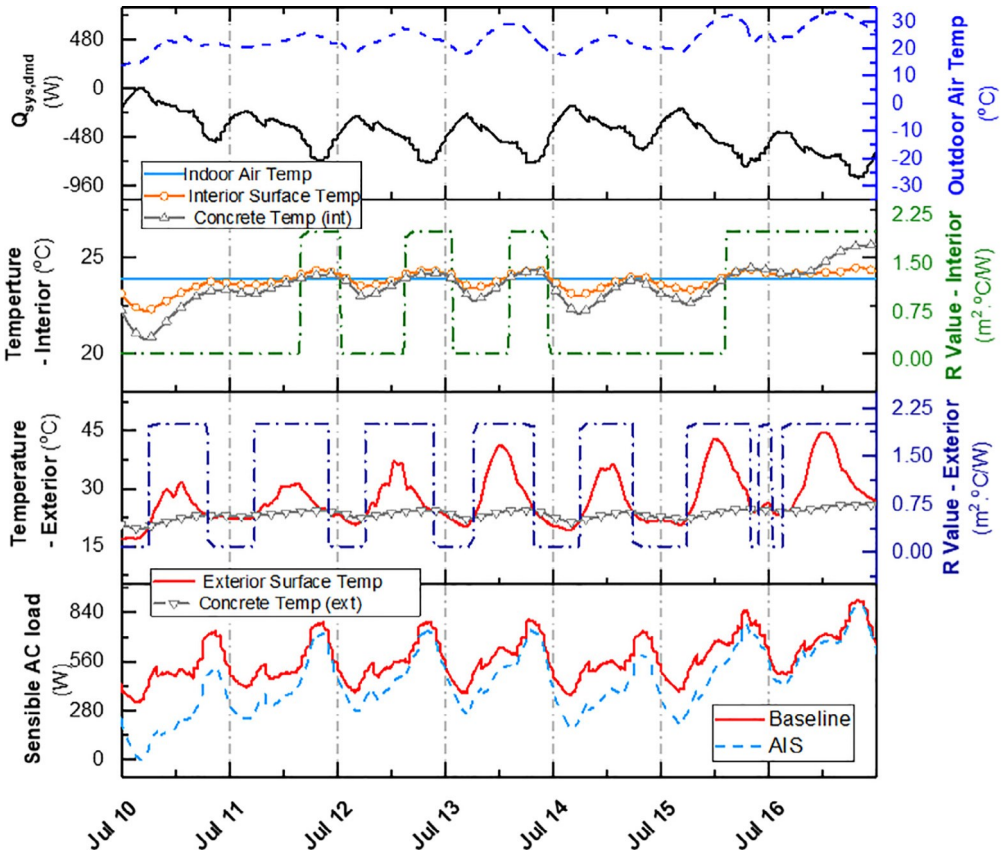

Fig. 6. Thermal behavior of RBE in a typical cooling season (July, Chicago, IL): (a) outdoor air temperature and the system output demand to reach the setpoint, $Q_{sys,dmd}$ (Equation (21)); (b) interior AIS RSI-value setting and indoor air, interior surface and concrete temperatures; (c) exterior AIS RSI-value setting, exterior surface and concrete temperatures; (d) comparison of sensible AC load for RBE and baseline cases.

a summer week (July 10th–16th) in Chicago, IL is selected to illustrate the how the RBE responds to the changes in outdoor environment. As indicated in Fig. 6 (a), the outdoor air temperature fluctuates around the AC set point, whereas the exterior surface temperature is mostly higher than the setpoint (23.9 C) due to solar irradiation during the daytime. Fig. 6(b) shows that when the temperature of concrete thermal mass is higher than the indoor air temperature, the interior AIS is at a low thermal conductivity (high thermal resistance). Whereas, when the temperature of concrete interior surface is lower than indoor air temperature, the concrete layer provides potential to absorb the unwanted heat from the indoor space. In that case, the controller first makes a determination if cooling from the HVAC is needed ($Q^{j}_{sys;dmd}$<0) and then the thermal resistance of interior AIS is adjusted according to Equation (25) to allow just enough heat flow to compensate the AC demand. Since in the summer (July), cooling is required for most hours with relatively high AC demand ($Q^{j}_{sys;dmd}$), the interior AIS remains at R_{low} for most of the time when free ambient cooling is available. This is different from the system behavior during transitional seasons as will be shown in following section. As shown in Fig. 6(c), when the exterior surface temperature is higher than the concrete layer, the thermal resistance of the exterior AIS is set to R_{high} to cut off the undesired heat flow into the thermal mass layer; whereas when the exterior surface temperature is lower than the concrete layer, the thermal resistance of the exterior AIS is set to R_{low} to dissipate the unwanted heat stored in the thermal mass during the cool hours (from midnight to early morning). In July, the exterior surface temperature of exterior AIS is mostly higher than the concrete temperature, providing limited free ambient cooling. Fig. 6(d) presents the comparison of the sensible AC load between RBE and baseline cases, where the RBE reduces energy consumption by 20 %during the hot summer month (July) in Chicago, IL.

5.2.3. Transitional season

Fig. 7 shows the thermal behavior and AIS settings for the RBE during a transitional season, where a representative week (April 16th – 22nd) in Chicago, IL was presented to illustrate how the dynamic RBE utilizes natural heating/cooling from outdoor environment to reduce AC load. During the simulated period, cooling demand (see Fig. 7(a)) dominates ($Q^{j}_{sys;dmd}$ < 0 and sensible AC load > 0) from April 16th to April 19th. Because of the relatively high outdoor air temperature (19 C–31 C) during April 16th to April 18th, the system demand was similar to that during the cooling season. In response, the interior AISs behaved as a thermal switch with its thermal resistance setting to R_{low} when the interior concrete temperature was lower than indoor air temperature during early mornings. The exterior AIS was also set to R_{low} to provide passive cooling during nights and early mornings to dissipate the unwanted heat stored in the thermal mass, see Fig. 7(c). As the outdoor air temperature gradually decreased from April 19th, both exterior and interior AISs were set to R_{low} to help dissipate the undesired heat. Consequently, AC load with RBE was largely reduced compared with the baseline, see Fig. 7(d).

During April 20th-21st, due to the passive cooling provided by the RBE, the indoor air temperature decreased to values between the dual setpoints and AC system demand $Q^{j}_{sys;dnd}$ stayed around zero. As a result, the interior AIS remained inactive during this time. As the indoor air temperature is getting close to the heating setpoint, the controller detected the potential actions based on the

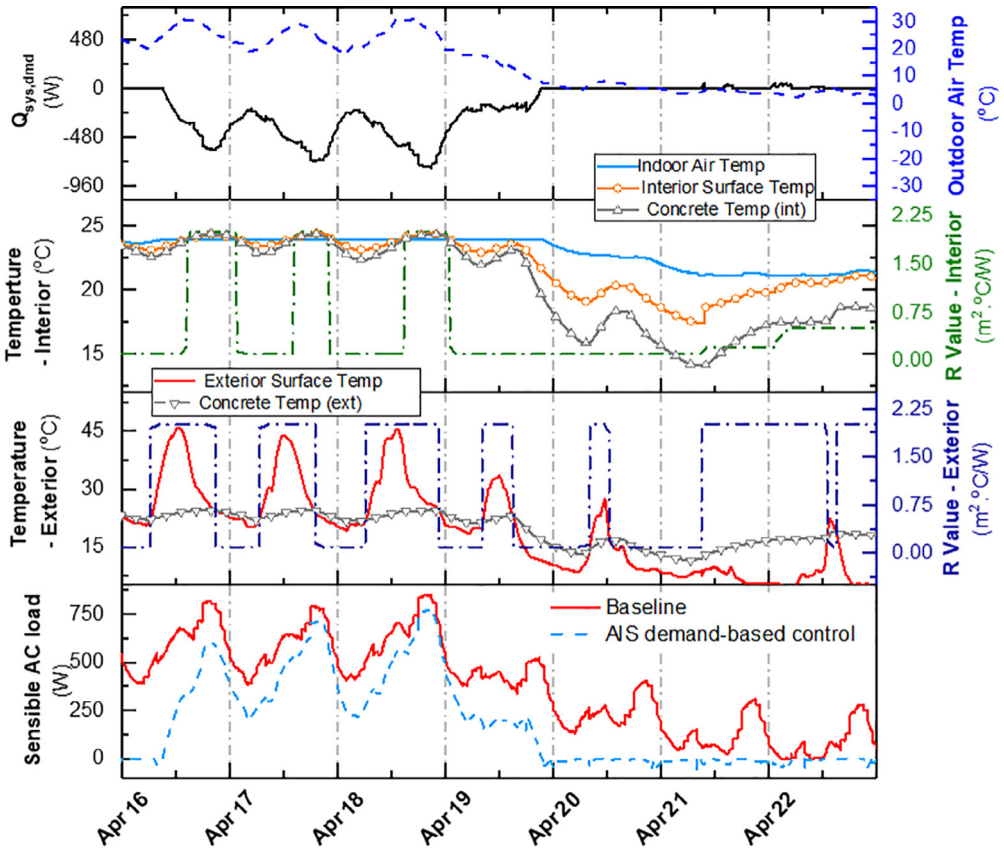

Fig. 7. Thermal behavior of RBE in a typical transitional season (April, Chicago, IL): (a) outdoor air temperature and the system output demand to reach the setpoint, $Q_{sys,dmd}$ (Equation (21)); (b) interior AIS RSI-value setting and indoor air, interior surface and concrete temperatures; (c) exterior AIS RSI-value setting, exterior surface and concrete temperatures; (d) comparison of sensible AC load for RBE and baseline cases.

gradually increased system demand (heating demand) around noon of April 21st. In response to the changes in the estimated system demand, the interior AIS gradually increased to a low level according to Equation (25) and maintains the system demand close to zero. During the morning of April 22nd, the projected system demand became positive again so that the interior AIS was gradually set to 0.5 Km^2/W based on Equation (25) and maintained as the same value as the system demand reached zero. The demand-based control rule developed in this research suppresses the AC demand via sensitive detection of potential changes to maintain the sensible AC load around zero during April 20th to April 22nd as compared to the high sensible AC load of baseline. The simulation results show that the RBEs brought approximately 75 %energy savings as compared to the RSI-4 static envelope baseline in April in Chicago, IL. Also, it is worth noting that due to the demand change (from cooling to heating) during the morning of April 21st, the control of exterior AIS automatically switched mode such that exterior AIS adjusted to R_{high} when the temperature of concrete continues to decrease. This helps prevent 'overcooling', which would in turn increase the AC energy usage. More detailed comparison between the 'demand-based' control rule as proposed in this research and temperature-based control will be elaborated in the following section.

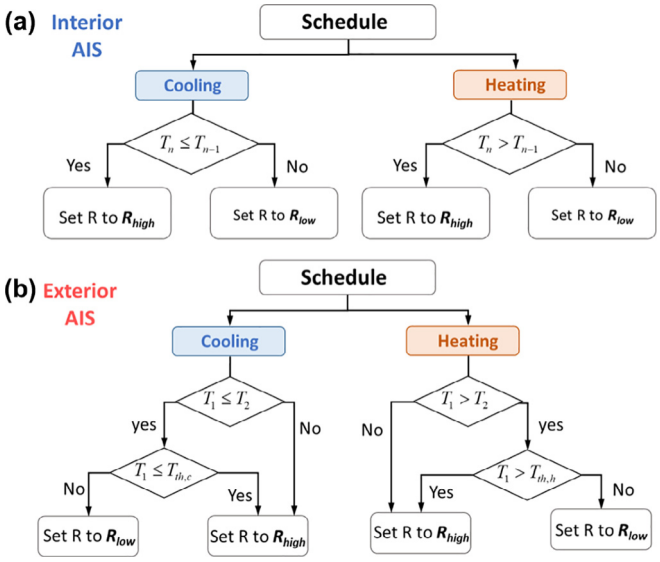

Fig. 8. Illustrative figure showing the temperature-based control rule (a) without, and (b) with threshold temperature (T_{th}).

5.2.4. Comparison with temperature -based control

In this section, the performance of the proposed demand-based control method for RBE is compared with temperature-based control rules. In particular, the temperature-based control rule shown as the block diagram in Fig. 8, is applied to the interior and exterior AISs. It was found in the previous work [15] that during transitional seasons, temperature-based control rules without a secondary temperature constraint tend to cause overcooling/overheating, especially in the case of AIS working together with a thermal mass. For example, during October in Chicago, IL, the baseline case (i.e., static envelope) requires mostly cooling due to the internal loads and relatively mild outdoor temperature. However,

the application of temperature-based controller without a secondary temperature restriction leads to ''over-cooling" during days when night temperatures are low (e.g., Oct 7th–9th, and Oct. 13th–21st), see Fig. 9(a). To prevent overcooling/overheating, some previous research proposed to apply a 'secondary rule' to regulate the temperature of the thermal mass [15] – e.g., during cooling season, if concrete temperature falls below a threshold value $T_{th,c}$, the exterior AIS is set to R_{high} in order to prevent overcooling.

Fig. 9 presents the thermal behavior (R setting) of RBEs controlled by different control rules, where Fig. 9(a) shows the temperature-based control without overcooling prevention in comparison with the cases with secondary temperature constraints (i.e., $T_{th,c}$ = 10 C, 16 C, and 22 C). The temperature of the thermal mass is regulated within a certain range by limiting the exterior surface temperature – i.e., when the exterior surface temperature of the envelope falls below $T_{th,c}$, the exterior AIS is set to R_{high}. While effective, a major limitation of this controller is that the system performance (e.g., energy saving potential) is highly dependent on the prescribed $T_{th,c}$, whose 'optimal' value varies dramatically based on the building configuration (e.g., internal load, AC setpoint etc.), specific weather condition, and even the system design. This is demonstrated in Fig. 9(b), where it can be seen that the energy saving maximizes when $T_{th,c}$ is between 10 and 16 C for October in Chiacago, IL. Note that the optimal value of $T_{th,c}$ leading to maximum saving potential varies month-to-month and is different for each climate zone. Therefore, the design of temperature rule controllers relies on high fidelity case analysis which is not always available. On the other hand, the proposed demand-based controller regulates AIS behaviors based on projected cooling/heating demand (i.e., Equation (21)). When the projected AC load is low, the actions of AIS are limited to automatically prevent overheating or overcooling from occurring, see Fig. 9(a). When the thermal mass temperature deviates too much from the desired cooling/heating temperature, the estimated AC demand will become non-zero to automatically trigger the action of AISs. This ensures the thermal mass stores and releases thermal energy just ''as-needed" and do no reply on a prescribed temperature constraint for control. Note that Equation (21) 'project' heating/cooling demand from AC based on current state of the building (i.e., measure surface, air temperatures, the estimated internal load and infiltration based on the occupancy schedule) and do not rely on a model to predict energy demand (as oppose to 'model predictive control, or MPC [26]'), which greatly simplifies the controller formulation. Moreover, this strategy triggered by system demand, as outlined in Fig. 3, reduces unnecessary actuation of AIS. This is advantageous as compared to most existing temperature driven control rule by providing effective 'on-demand' shedding of AC load while reducing the operational energy and maintenance requirement at the same time.

5.3. Energy saving potential and operation

5.3.1. Energy saving potential and thermal comfort performance in different climate zones

Fig. 10 shows the monthly and annual energy consumption from the AC cooling/heating (including sensible load and latent load) of the analyzed thermal zone located in Miami, Phoenix, San Francisco, Albuquerque, Chicago, and Minneapolis, which are in ASHREA climate zones 1A, 2B, 3C, 4B, 5A, and 6A-7, respectively. The energy saving potentials of the RBE with the two different control rules – i.e., temperature-based control (with $T_{th,c}$ = 16 C and $T_{th,h}$ = 30 C based on prior analysis performed by Kishore et al. [15]) and demand-based control, are also compared. The simulation results indicate that AC load was significantly reduced by the RBEs in most thermal zones regardless of the controller used. Dynamic envelope is demonstrated to be very effective in reducing AC load in climate zones with relatively mild climate and during transitional reasons – e.g., over 90 % energy savings can be achieved in San Francisco, CA or during winter months of Albuquerque, see Fig. 10(a); whereas RBE has limited saving potential for hot summers or cold winters when the outdoor temperature is constantly above or below the indoor temperatures (e.g., summer of Miami or winter of Minneapolis). This trend is consistent with results presented in previous studies [22]. Overall, the simulation results show that the RBE with AIS under demand-based control provided up to 32.0 %higher energy savings than the one under temperature-based control. The higher saving potential brought by the demand-based control rule is more evident in climate zones with mild climate or during transitional seasons. This is due to the high diurnal and monthly temperature fluctuations that lead to overcooling or overheating as discussed in previous sections.

In addition, the thermal comfort performance was also calculated for the baseline and RBE cases under both temperature-based control and under demand-based control. Table 1 presents the annual Long-term Percentage of Dissatisfied (LPD) for these

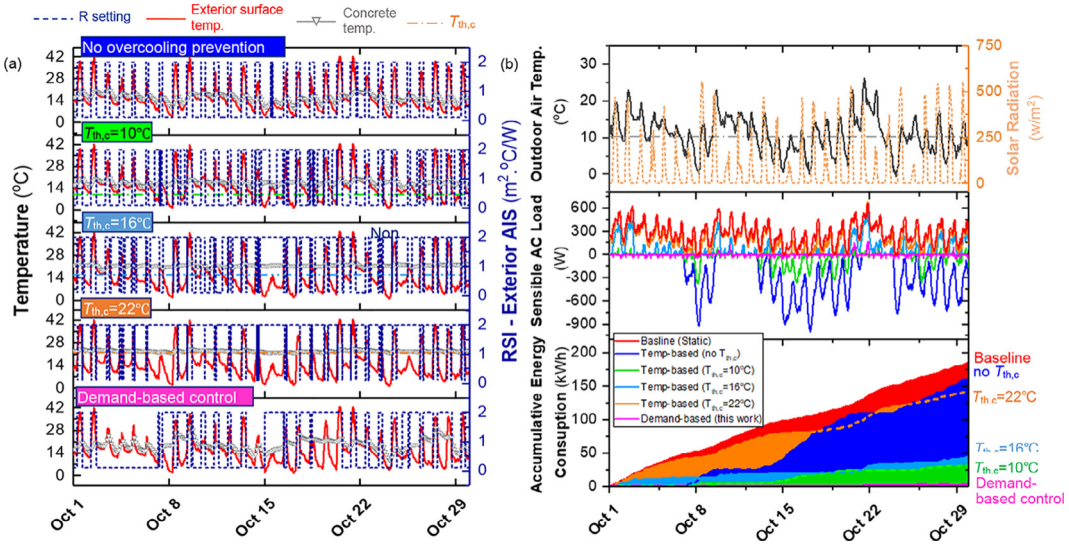

Fig. 9. Comparison of RBE thermal behavior under demand-based control and temperature-based control.

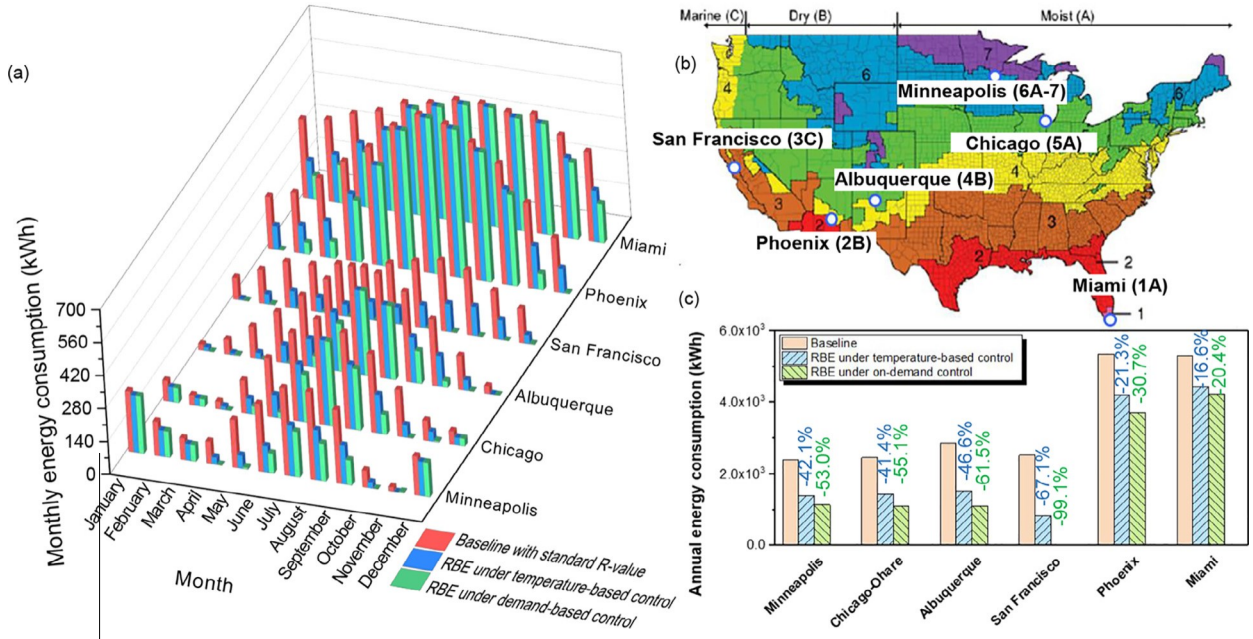

Fig. 10. (a) Monthly energy consumption of the residential thermal zone (b) Climate classification of the six representative cities analyzed (c) Annual energy consumption compared for the static envelope baseline, RBE with temperature-based control, and RBE with demand-based control.

Table 1
The annual LPD (%) of the residential thermal zone in different scenarios.

	Miami (1A)	Phoenix (2B)	San Francisco (3C)	Albuquerque (4B)	Chicago (5A)	Minneapolis (6A-7)
Baseline	9.19	7.54	8.08	6.98	7.88	8.00
RBE under temperature-based control	8.98 (2.2 %)	7.38 (2.1 %)	7.79 (3.6 %)	6.85 (1.9 %)	7.50 (4.9 %)	7.73 (3.3 %)
RBE under demand-based control	8.83 (3.9 %)	7.05 (6.4 %)	5.89 (27.1 %)	6.57 (5.9 %)	7.14 (9.4 %)	7.37 (7.9 %)

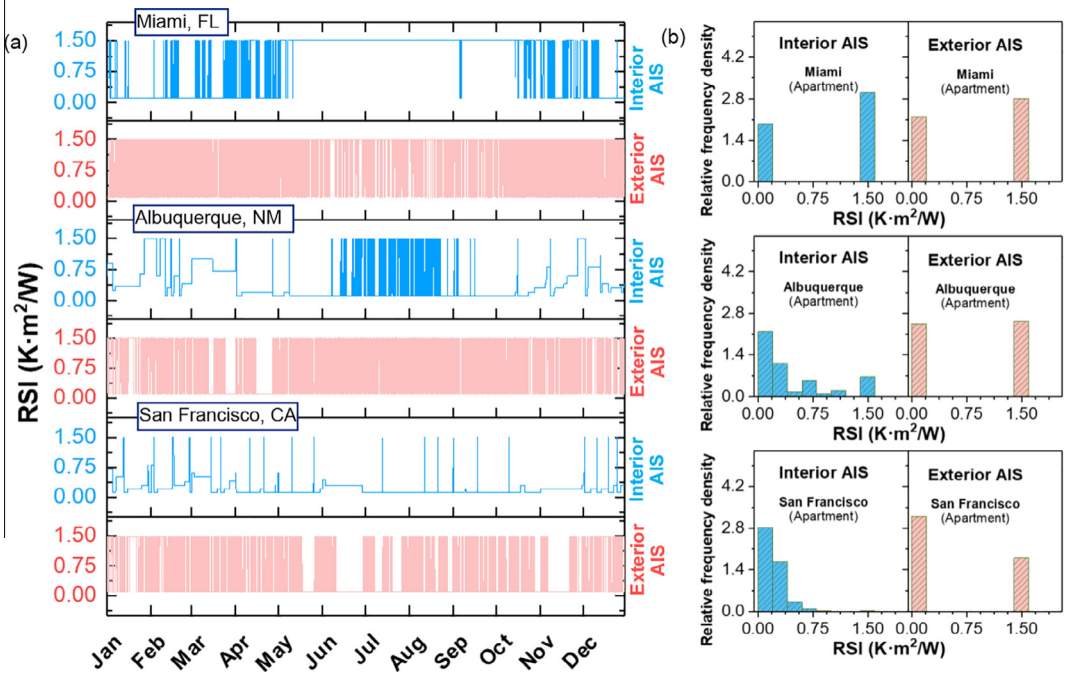

Fig. 11. (a) Whole-year time history of RSI setting for both the interior and exterior AIS for Miami, Albuquerque, and San Francisco; (b) Relative frequency density distribution of the RSI-values.

three cases in the 6 representative cities. The simulation results indicate that RBE can maintain satisfactory thermal comfort performance while providing energy savings. The RBE using demand-based control provides higher LPD reductions as compared to those using temperature-based control, especially in regions with relative mild climate (i.e., San Francisco).

5.3.2. Operation of AIS and design implications

Fig. 11(a) presents the time histories of RSI-value of the AISs during a meteorological year under the demand-based control. During the hot summer months (i.e., May–October) in Miami, the interior AIS mostly stays at R_{high} to minimize the undesirable heat flowing into the indoor space while the exterior AIS still goes through daily transitions to dissipate the heat stored in the thermal mass during evening cooler hours. For Albuquerque, the interior AIS hovered mostly at lower insulation levels during winter and traditional seasons to utilize passive heating/cooling and reduce AC load. In regions with mild climate like San Francisco, the interior AIS mostly stayed at very low insulation levels.

Fig. 11(b) presents the relative (time) frequency density distribution of the RSI-value of both interior and exterior AIS for three climate zones – Miami (1A), Albuquerque (4B), and San Francisco (3C). It can be seen that for Miami, the interior and exterior AISs mostly switches between the highest and lowest RSI-values R_{low} and R_{high} throughout the year and it rarely stay at intermediate RSI-value. This indicates that for regions with predominantly hot or cold seasons, AIS designs that switch between R_{low} and R_{high}, or sometimes been referred as to ‘‘binary thermal switch” [23], could yield ‘near-optimal’ performance. Whereas for areas with longer transitional seasons (e.g., Albuquerque), AISs that can ‘gradually’ change their thermal resistance can provide higher energy saving potential. It also can be observed from the results that for areas with mild climate (e.g., San Francisco), only relatively low interior insulation level is needed – i.e., the RSI-value of interior AIS stayed mostly <0.5 Km^2/W throughout the year, therefore, the RBE designed with only exterior AIS may provide satisfactory energy performance. The results of thermal insulation duration distribution can help to determine the suitable AIS type and required insulation level for AIS design in different climate zones.

6. Conclusions and future outlook

Although it has been well demonstrated that responsive building envelope (RBE) has tremendous potential to improve building’s energy performance by dynamically providing passive cooling/heating to reduce energy consumption, there is still significant gap in formulating the control strategy of such systems. In particular, for RBEs that integrate active insulation systems (AISs) and thermal energy storage (TES), the formulation of optimal control rule of such system is challenging. In this research, an easy-to-implement yet flexible ‘demand-based’ control rule is formulated for the TES-AIS integrated RBEs to beneficially utilize the heat storage capacity or precooling of the thermal mass to reduce AC load. The control rule is formulated by first estimating AC demand from estimated internal gains, infiltration, as well as measured surface temperatures and air temperatures at certain time steps. Then the desired thermal resistance of AIS is calculated based on the estimated AC demand and temperatures of the thermal mass and indoor air. To evaluate the performance of the RBE system with demand-based control, a thermal network model was formulated to simulate thermal zones that are equipped with a RBE exterior wall. Case studies were conducted in six (6) climate zones. The key findings of the study are summarized below:

In comparison to temperature-based control strategies in prior studies, the demand-based control rule formulated herein has achieved significantly higher energy saving potential. During transitional seasons, the temperature-based controller tends to cause overheating or overcooling of the thermal mass which largely limits the energy saving potential of RBEs; whereas the demand-based controller ensures that the AISs release thermal energy just ‘‘as-needed” and do no reply on a prescribed temperature constraint for control. For regions with mild climate, e.g., San Francisco, the demand-based control reduces the AC energy consumption by over 90 %. The RBEs also bring thermal comfort improvement especially for regions with mild climate condition (e.g., 27.1 % LPD reduction in San Francisco, CA).

A thermal network model with high computational efficiency is established for RBEs with integrated AISs and TES (or high thermal mass). The thermal performance (e.g., temperature responses and energy consumptions) matches closely with those obtained by EnergyPlus simulations. The higher efficiency model is important to reduce computational costs for further studies that employ AI-based or online learning control.

The integrated TES-AIS RBE has significant potential to reduce the energy consumption of buildings located in most climate zones. In particular, the case study had shown 20.4 %, 30.7 %, 99.1 %, 61.5 %, 55.1, and 53.0 % heating/cooling energy use reductions for Miami (1A), Phoenix (2B), San Francisco (3C), Albuquerque (4B), Chicago (5A), and Minneapolis (6A-7), respectively. The responses from AIS systems help charge and discharge the thermal mass and provide compensating heat flow to offset the AC load. In general, the energy saving potential of RBE is greater during transitional seasons and in regions with mild climate where the diurnal temperature fluctuates around the AC set points.

The analysis of whole-year AIS operation across different climate zones can provide guidance for AIS design. It was found that for regions with predominantly hot or cold climate, the use of ‘‘two-step” thermal switch would yield satisfactory thermal performance; whereas for regions with long transitional seasons, AISs that can gradually change their thermal resistance can provide higher energy saving potential. In addition, for regions with mild climate (e.g., San Francisco), RBE with only exterior AIS (interior side is not insulated) can provide satisfactory performance.

Some limitations and future outlook of the current study include:

The control approach discussed herein was formulated and applicable to only a single thermal zone. Control strategies and design optimizations for RBE implementation in multi-thermal zone buildings are needed for future studies.

RBE controls can be oriented towards multiple objectives including grid flexibility, air quality, and daylighting performance, other than focusing sole on energy efficiency and thermal comfort. In addition, occupancy behavior can be integrated as part of RBE control.

Data-driven approaches including reinforcement learning control worth further investigation as they do not rely on physical models.

Data availability

Data will be made available on request.

Declaration of Competing Interest

The authors declare that they have no known competing financial interests or personal relationships that could have appeared to influence the work reported in this paper.

Acknowledgments

This research was made possible by National Science Foundation (CMMI-1663302, CMMI-1954517). The funding support from NSF is greatly appreciated.

References

[1] Wigginton M, Harris J. Intelligent Skins. 2002.

[2] N. Biloria, V. Sumini, Performative building skin systems: a morphogenomic approach towards developing real-time adaptive building skin systems, Int J Archit Comput 7 (2009) 643–675, https://doi.org/10.1260/1478-0771.7.4.643.

[3] J. Joe, W. Choi, H. Kwon, J.H. Huh, Load characteristics and operation strategies of building integrated with multi-story double skin facade, Energy Build 60 (2013) 185–198, https://doi.org/10.1016/j.enbuild.2013.01.015.

[4] R.C.G.M. Loonen, M. Trčka, D. Cóstola, J.L.M. Hensen, Climate adaptive building shells: state-of-the-art and future challenges, Renew Sustain Energy Rev 25 (2013) 483–493, https://doi.org/10.1016/j.rser.2013.04.016.

[5] Loonen RCGM. Bio-inspired Adaptive Building Skins. In: F. Pacheco Torgal, J.A. Labrincha, M.V. Diamanti, C.P. Yu, H.K. Lee, editors. Biotechnol. Biomimetics Civ. Eng., Springer; 2015, p. 115–34.

[6] W.J. Stec, A.H.C. van Paassen, Symbiosis of the double skin facade with the HVAC system, Energy Build 37 (2005) 461–469, https://doi.org/10.1016/j.enbuild.2004.08.007.

[7] A. Athienitis, W.O. Brien, Modeling, design, and optimization of net-zero, Energy Build. (2015).

[8] E. Taveres-Cachat, S. Grynning, J. Thomsen, S. Selkowitz, Responsive building envelope concepts in zero emission neighborhoods and smart cities - A roadmap to implementation, Build Environ 149 (2019) 446–457, https://doi.org/10.1016/j.buildenv.2018.12.045.

[9] K.T.G. Velikov, Responsive building envelopes: characteristics and evolving paradigms, Des. Constr. High-Performance Homes (2013) 75–92.

[10] X. Xu, D.S. Van, A. Messac, Study of the performance of thermoelectric modules for use in active building envelopes, Build. Environ. 42 (2007) 1489–1502, https://doi.org/10.1016/j.buildenv.2005.12.021.

[11] X. Xu, D.S. Van, Evaluation of an active building envelope window-system, Build. Environ. 43 (2008) 1785–1791, https://doi.org/10.1016/j.buildenv.2007.10.013.

[12] Jong-Jin Kim, Jin Woo Moon. IMPACT OF INSULATION ON BUILDING ENERGY CONSUMPTION. Elev. Int. IBPSA Conf., 2009, p. 674–80.

[13] V. Cheng, E. Ng, B. Givoni, Effect of envelope colour and thermal mass on indoor temperatures in hot humid climate, Sol. Energy 78 (2005) 528–534, https://doi.org/10.1016/j.solener.2004.05.005.

[14] A. Reilly, O. Kinnane, The impact of thermal mass on building energy consumption, Appl. Energy 198 (2017) 108–121, https://doi.org/10.1016/j.apenergy.2017.04.024.

[15] R.A. Kishore, M.V.A. Bianchi, C. Booten, J. Vidal, R. Jackson, Enhancing building energy performance by effectively using phase change material and dynamic insulation in walls, Appl. Energy 283 (2021), https://doi.org/10.1016/j.apenergy.2020.116306 116306.

[16] B. Park, W.V. Srubar, M. Krarti, Energy performance analysis of variable thermal resistance envelopes in residential buildings, Energy Build. 103 (2015) 317–325, https://doi.org/10.1016/j.enbuild.2015.06.061.

[17] K. Menyhart, M. Krarti, Potential energy savings from deployment of Dynamic Insulation Materials for US residential buildings, Build. Environ. 114 (2017) 203–218, https://doi.org/10.1016/j.buildenv.2016.12.009.

[18] V. Shekar, M. Krarti, Control strategies for dynamic insulation materials applied to commercial buildings, Energy Build. 154 (2017) 305–320, https://doi.org/10.1016/j.enbuild.2017.08.084.

[19] A.H.A. Dehwah, M. Krarti, Impact of switchable roof insulation on energy performance of US residential buildings, Build. Environ. 177 (2020), https://doi.org/10.1016/j.buildenv.2020.106882 106882.

[20] S. Rupp, M. Krarti, Analysis of multi-step control strategies for dynamic insulation systems, Energy Build. 204 (2019), https://doi.org/10.1016/j.enbuild.2019.109459.

[21] M. Juaristi, F. Favoino, T. Gómez-Acebo, A. Monge-Barrio, Adaptive opaque façades and their potential to reduce thermal energy use in residential buildings: a simulation-based evaluation, J. Build. Phys. (2021), https://doi.org/10.1177/17442591211045418.

[22] F. Antretter, P. Boudreaux, Assessing the potential of active insulation systems to reduce energy consumption and enhance electrical grid services, 2019 Build. XIV Int. Conf. (2019) 12–15.

[23] S. Mumme, N. James, Smart and efficient building envelopes: thermal switches and thermal storage for energy savings and load flexibility, ASHRAE Trans. 126 (2020) 140–148.

[24] F. Favoino, Q. Jin, M. Overend, Design and control optimisation of adaptive insulation systems for office buildings. Part 1: adaptive technologies and simulation framework, Energy 127 (2017) 301–309, https://doi.org/10.1016/j.energy.2017.03.083.

[25] Q. Jin, F. Favoino, M. Overend, Design and control optimisation of adaptive insulation systems for office buildings. Part 2: a parametric study for a temperate climate, Energy 127 (2017) 634–649, https://doi.org/10.1016/j.energy.2017.03.096.

[26] B. Cui, J. Dong, S. Lee, P. Im, M. Salonvaara, D. Hun, et al., Model predictive control for active insulation in building envelopes, Energy Build. 267 (2022), https://doi.org/10.1016/j.enbuild.2022.112108 112108.

[27] J. Ma, S.J. Qin, T. Salsbury, Application of economic MPC to the energy and demand minimization of a commercial building, J. Process Control 24 (2014) 1282–1291, https://doi.org/10.1016/j.jprocont.2014.06.011.

[28] E. Biyik, A. Kahraman, A predictive control strategy for optimal management of peak load, thermal comfort, energy storage and renewables in multi-zone buildings, J. Build. Eng. 25 (2019), https://doi.org/10.1016/j.jobe.2019.100826 100826.

[29] M.J. Bursill, L. O'Brien, I. Beausoleil-Morrison, Multi-zone field study of rule extraction control to simplify implementation of predictive control to reduce building energy use, Energy Build. 222 (2020), https://doi.org/10.1016/j.enbuild.2020.110056 110056.

[30] M. Gholamzadehmir, C. Del Pero, S. Buffa, R. Fedrizzi, N. Aste, Adaptive-predictive control strategy for HVAC systems in smart buildings – A review, Sustain. Cities Soc. 63 (2020), https://doi.org/10.1016/j.scs.2020.102480.

[31] P.H. Shaikh, N.B.M. Nor, P. Nallagownden, I. Elamvazuthi, T. Ibrahim, A review on optimized control systems for building energy and comfort management of smart sustainable buildings, Renew. Sustain. Energy Rev. 34 (2014) 409–429, https://doi.org/10.1016/j.rser.2014.03.027.

[32] J.M. Santos-Herrero, J.M. Lopez-Guede, I. Flores-Abascal, Modeling, simulation and control tools for nZEB: a state-of-the-art review, Renew. Sustain. Energy Rev. 142 (2021), https://doi.org/10.1016/j.rser.2021.110851 110851.

[33] T. Pflug, T.E. Kuhn, R. Nörenberg, A. Glück, N. Nestle, C. Maurer, Closed translucent façade elements with switchable U-value - A novel option for energy management via the facade, Energy Build. 86 (2015) 66–73, https://doi.org/10.1016/j.enbuild.2014.09.082.

[34] T. Pflug, N. Nestle, E.T. Kuhn, M. Siroux, C. Maurer, Modeling of facade elements with switchable U-value, Energy Build. 164 (2018) 1–13, https://doi.org/10.1016/j.enbuild.2017.12.044.

[35] R.C.G.M. Loonen, P. Hoes, J.L. Hensen. Performance prediction of buildings with responsive building elements: challenges and solutions. Proc. Build. Simul. Optim. 2014 1–8.

[36] J.A. Tomko, A. Pena-Francesch, H. Jung, M. Tyagi, B.D. Allen, M.C. Demirel, et al., Tunable thermal transport and reversible thermal conductivity switching in topologically networked bio-inspired materials, Nat. Nanotechnol. 13 (2018) 959–964, https://doi.org/10.1038/s41565-018-0227-7.

[37] D.K. Benson, T.F. Potter, C.E. Tracy, Design of a variable-conductance vacuum insulation, SAE Tech. Pap. 103 (1994) 176–181, https://doi.org/10.4271/940315.

[38] Z. Wu, Z. Feng, B. Sunden, L. Wadsoe, A comparative study on thermal conductivity and rheology properties of alumina and multi-walled carbon nanotube nanofluids, Front. Heat Mass Transf. 5 (2014), https://doi.org/10.5098/hmt.5.18.

[39] S. Varga, A.C. Oliveira, C.F. Afonso, Characterisation of thermal diode panels for use in the cooling season in buildings, Energy Build. 34 (2002) 227–235, https://doi.org/10.1016/S0378-7788(01)00090-1.

[40] M. Kimber, W.W. Clark, L. Schaefer, Conceptual analysis and design of a partitioned multifunctional smart insulation, Appl. Energy 114 (2014) 310–319, https://doi.org/10.1016/j.apenergy.2013.09.067.

[41] ASHRAE. ANSI/ASHRAE/IEC Standard 90.1-2019: Energy Standard for Buildings Except Low-Rise Residential Buildings. 2019.

[42] Council NFR. National Fenestration Rating Council Incorporated NFRC 700-2013[E1A1] Product Certification Program 2013.

[43] L. Berkeley, O.A.K. Ridge, M.B.Y. Ut-battelle, A. For, S. Energy, D. Or, et al. EnergyPlusTM Version 8.9.0 Documentation Input Output Reference. 2019.

[44] ADVANCED RESEARCH PROJECTS AGENCY – ENERGY (ARPA-E) U.S. DEPARTMENT OF ENERGY. DELIVERING EFFICIENT LOCAL THERMAL AMENITIES (DELTA),DE-FOA-0001127. 2014.

[45] D. Kim, J.E. Braun, A general approach for generating reduced-order models for large multi-zone buildings, J. Build. Perform. Simul. 8 (2015) 435–448, https://doi.org/10.1080/19401493.2014.977952.

[46] Y. He, Y. Zhang, C. Zhang, H. Zhou, Energy-saving potential of 3D printed concrete building with integrated living wall, Energy Build. 222 (2020), https://doi.org/10.1016/j.enbuild.2020.110110 110110.

[47] J.W. Deardorff, Efficient prediction of ground surface temperature and moisture, with inclusion of a layer of vegetation, J. Geophys. Res. 83 (1978) 1889, https://doi.org/10.1029/jc083ic04p01889.

[48] L. Berkeley, O.A.K. Ridge, M.B.Y. Ut-battelle, A. For, S. Energy, D. Or, et al. EnergyPlus™ Version 8.9.0 Documentation Engineering Reference. 2019.

[49] V. Monetti, E. Davin, E. Fabrizio, P. André, M. Filippi, Calibration of building energy simulation models based on optimization: a case study, Energy Procedia 78 (2015) 2971–2976, https://doi.org/10.1016/j.egypro.2015.11.693.

[50] Z. Li, J. Zhang, Study on the distributed model predictive control for multi-zone buildings in personalized heating, Energy Build 231 (2021), https://doi.org/10.1016/j.enbuild.2020.110627 110627.

[51] P.D. Moroan, R. Bourdais, D. Dumur, J. Buisson, Building temperature regulation using a distributed model predictive control, Energy Build 42 (2010) 1445–1452, https://doi.org/10.1016/j.enbuild.2010.03.014.

[52] A. Berge, C.E. Hagentoft, P. Wahlgren, B. Adl-Zarrabi, Effect from a variable U-Value in Adaptive building components with controlled internal air pressure, Energy Procedia 78 (2015) 376–381, https://doi.org/10.1016/j.egypro.2015.11.677.

[53] ISO, ISO 7730: Ergonomics of the thermal environment Analytical determination and interpretation of thermal comfort using calculation of the PMV and PPD indices and local thermal comfort criteria, Management 3 (2005) 605–615, https://doi.org/10.1016/j.soildyn.2004.11.005.

[54] S. Carlucci. Thermal Comfort Assessment of Buildings. Springer Milan Heidelberg New York Dordrecht London; 2013. https://doi.org/10.1007/978-88-470-5238-3.